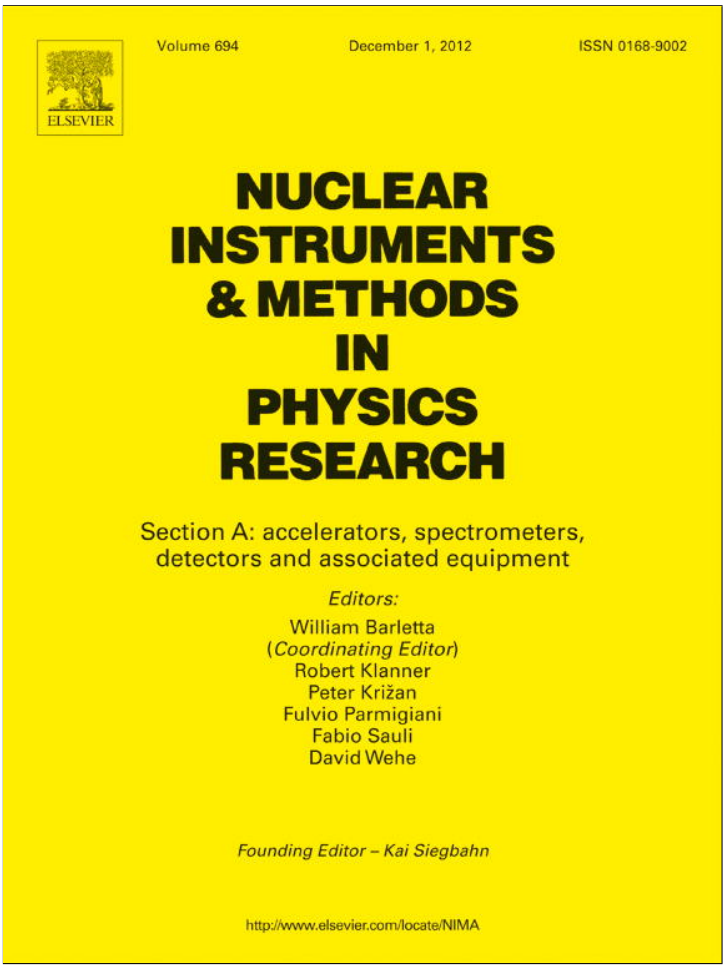

Nuclear Instruments and Methods in Physics Research A 694 (2012) 55–68

Contents lists available at SciVerse ScienceDirect

Nuclear Instruments and Methods in Physics Research A

journal homepage: www.elsevier.com/locate/nima

Characterization of extended range Bonner Sphere Spectrometers in the CERF high-energy broad neutron field at CERN

S. Agosteo [a], R. Bedogni [b], M. Caresana [a], N. Charitonidis [c,d], M. Chiti [b], A. Esposito [b], M. Ferrarini [a,e], C. Severino [c,f,1], M. Silari [c,*]

[a] Politecnico di Milano, Dipartimento di Energia, Via Ponzio 34/3, 20133 Milano, Italy
[b] INFN-LNF, Laboratori Nazionali di Frascati, Via Fermi 40, 00044 Frascati, Italy
[c] CERN, 1211 Geneva 23, Switzerland
[d] École Polytechnique Fédérale de Lausanne (EPFL), CH-1015 Lausanne, Switzerland
[e] Fondazione CNAO, Strada Campeggi 53, 27100 Pavia, Italy
[f] Istituto Universitario di Studi Superiori di Pavia, IUSS, Viale Lungo Ticino Sforza 56, 27100 Pavia, Italy

ARTICLE INFO

Article history:
Received 1 March 2012
Received in revised form
21 June 2012
Accepted 23 June 2012
Available online 7 August 2012

Keywords:
Neutron spectrometry
Bonner spheres
Neutron spectra unfolding
Radiation protection

ABSTRACT

The accurate determination of the ambient dose equivalent in the mixed neutron–photon fields encountered around high-energy particle accelerators still represents a challenging task. The main complexity arises from the extreme variability of the neutron energy, which spans over 10 orders of magnitude or more. Operational survey instruments, which response function attempts to mimic the fluence-to-ambient dose equivalent conversion coefficient up to GeV neutrons, are available on the market, but their response is not fully reliable over the entire energy range. Extended range rem counters (ERRC) do not require the exact knowledge of the energy distribution of the neutron field and the calibration can be done with a source spectrum. If the actual neutron field has an energy distribution different from the calibration spectrum, the measurement is affected by an added uncertainty related to the partial overlap of the fluence-to-ambient dose equivalent conversion curve and the response function. For this reason their operational use should always be preceded by an "in-field" calibration, i.e. a calibration made against a reference instrument exposed in the same field where the survey-meter will be employed. In practice the extended-range Bonner Sphere Spectrometer (ERBSS) is the only device which can serve as reference instrument in these fields, because of its wide energy range and the possibility to assess the neutron fluence and the ambient dose equivalent ($H^*(10)$) values with the appropriate accuracy. Nevertheless, the experience gained by a number of experimental groups suggests that mandatory conditions for obtaining accurate results in workplaces are: (1) the use of a well-established response matrix, thus implying validation campaigns in reference monochromatic neutrons fields, (2) the expert and critical use of suitable unfolding codes, and (3) the performance test of the whole system (experimental set-up, elaboration and unfolding procedures) in a well controlled workplace field. The CERF (CERN-EU high-energy reference field) facility is a unique example of such a field, where a number of experimental campaigns and Monte Carlo simulations have been performed over the past years.

With the aim of performing this kind of workplace performance test, four different ERBSS with different degrees of validation, operated by three groups (CERN, INFN-LNF and Politecnico of Milano), were exposed in two fixed positions at CERF. Using different unfolding codes (MAXED, GRAVEL, FRUIT and FRUIT SGM), the experimental data were analyzed to provide the neutron spectra and the related dosimetric quantities. The results allow assessing the overall performance of each ERBSS and of the unfolding codes, as well as comparing the performance of three ERRCs when used in a neutron field with energy distribution different from the calibration spectrum.

1. Introduction

Neutrons may represent the dominant component in the stray radiation field outside the shielding of particle accelerators and contribute to most of the total ambient dose equivalent in accessible areas during accelerator operation [1]. The neutron

* Corresponding author. Tel.: +41 22 76 73937.
E-mail address: marco.silari@cern.ch (M. Silari).
[1] Now with CERN and the University of Bern, CH-3012, Bern, Switzerland.

0168-9002/$ - see front matter © 2012 Elsevier B.V. All rights reserved.
http://dx.doi.org/10.1016/j.nima.2012.06.055

spectrum extends from thermal energies up to a value that depends on various factors such as type and energy of the accelerated particles, target material and geometry, emission angle, shield material and thickness. As far as the dosimetric quantities are concerned, the neutron spectra at workplaces at high-energy accelerators show two important components: (1) an evaporation component, mainly due to particle–nucleus quasi-isotropic interactions and usually described with a maxwellian shaped peak with most probable energy in the MeV region and (2) a high-energy component ($E > 10$ MeV) due to particle–nucleon high-energy interactions and extending up to hundreds MeV. Because the cross-section of most shielding materials reaches a minimum at about 100 MeV, the high-energy component after thick shields tends to present a peak around this energy value. This component may account for a substantial fraction of the neutron dose equivalent, sometimes up to 40–50% [2].

The instrument normally employed in radiation protection for determining the neutron energy distributions at workplaces is the Bonner Sphere Spectrometer (BSS), introduced by Bramblett, Ewing and Bonner in 1960 [3]. A BSS consists of a set of moderating spheres (typically from 5 to 15 in number) of different sizes made of polyethylene, each with a thermal neutron counter (active or passive) at its center. Each detector (moderator plus counter) has a response function peaking at a given energy, which depends on the size of the sphere. The combination of all response functions is the response matrix of the BSS. A "conventional" BSS consisting of only polyethylene moderators has an inherent upper energy limit around 10–20 MeV. Fairly recently BSS have been developed to include one or more moderators made of a combination of polyethylene and a high-Z material (such as lead or copper) to extend the response matrix to hundreds MeV, following the same approach used 20 years ago in the development of the first extended range rem counter (ERRC), the LINUS [4,5]. The detection of high-energy neutrons in extended-range moderating instruments relies on the inelastic (n,xn) reactions that occur in the high-Z material and produce secondary lower-energy neutrons having higher probability to be further moderated and then detected in the central counter (see e.g. Refs. [6–12]. These systems are conventionally called Extended Range Bonner Sphere Spectrometers (ERBSS). The neutron spectrum is reconstructed by unfolding the experimental counts of the BSS with its response matrix.

In July 2010 an experimental campaign employing four different ERBSSs (three active and one passive) and three different ERRCs based on the LINUS design (the original LINUS, another active unit and a passive model) was conducted at the CERF (CERN-EU high-energy reference field) facility [13]. Two test positions on the concrete shielded measurement area (named CT7 and CT9) were chosen for this experiment. The three participating groups, CERN, INFN-LNF and the Politecnico of Milano (POLIMI), undertook the following tasks:

(1) Determination of the qualitative properties, such as the spectrum normalized to the unit fluence, $\varphi(E)$, the spectrum-average-fluence to ambient dose equivalent conversion coefficient, $h^*(10)$, the fluence-average energy, E_{φ}, and the fractions of neutron fluence comprised in given energy intervals of interest, namely: $E < 0.4$ eV (thermal component), $0.4\ \text{eV} < E < 10$ keV (epithermal), $10\ \text{keV} < E < 10$ MeV (evaporative/fast) and $E > 10$ MeV (high-energy component). To determine the neutron spectrum, the FRUIT, MAXED and GRAVEL unfolding codes were used. Advantages and disadvantages of the unfolding algorithms are discussed.
(2) Determination of the spectrum-integrated quantities such as the total neutron fluence, Φ, and the ambient dose equivalent, $H^*(10)$.
(3) Direct determination of the ambient dose equivalent, $H^*(10)$ with the ERRCs for comparison with the values deduced by the ERBSSs and the "reference" Monte Carlo value [13].

This paper provides an overview of the results of the analysis performed by the three groups and discusses how they compare with the simulated data, obtained in the past with the FLUKA code.

2. The reliability of transport codes in High-energy fields

Monte Carlo transport codes like MCNPX [14], FLUKA [15,16], GEANT [17] and PHITS [18], play a crucial role in neutron spectrometry and dosimetry because they are used to determine the response functions or the instruments as well as, in some cases, the reference spectra of irradiation facilities. Simulations data are usually reliable in the energy domain below 20 MeV, because evaluated cross-section data, like ENDF/B [19], are available. Some codes use more extended data sets, e.g. MCNPX uses cross-section data library up to 150 MeV. In addition the experimental groups can validate the simulated response of instruments in a variety of ISO reference neutron fields, either mono-energetic or broad-spectra. As a result, the typical overall uncertainty of a well-established BSS response matrix, calculated with one of the mentioned codes, is in the order of 3% in the energy range below 20 MeV [20,6]. At higher energies, especially above 150 MeV, measured cross-section data are scarcely available and the codes rely on nuclear models describing the high-energy inelastic interaction in terms of intra-nuclear cascade (INC), pre-equilibrium and de-excitation models. Validation experiments are difficult to organize because of the limited availability of quasi-monoenergetic fields with high metrological quality.

A variety of benchmarking tests have been performed, and new initiatives are planned in the framework of WG11 of EURADOS (the European Radiation Dosimetry Group [21]). Specific calculations have been carried out to assess the code-to-code variability in determining the response function of an ERBSS [22]. Simulation codes have been compared with experimental data on neutron production from targets at different energies and angles [23,24]. In all cases, discrepancies as large as a factor of two can be observed in specific benchmarking conditions. However, the overall impact of such differences on the determination of ambient dose equivalent, neutron fluence or fluence in broad energy intervals at workplaces is generally limited to $\pm 10\%$.

The above figure is confirmed by a recent experiment performed by the INFN-LNF group at TSL in Uppsala, Sweden. Here the high-energy fluence of the ANITA neutron beam, sharply peaked at about 180 MeV and previously known via fission-based reference instruments, was determined with a dysprosium foils-based ERBSS. The results agreed with the reference data within less than 10% (the uncertainty stated for the reference fluence was also 10%) [25]. Similar differences in terms of $H^*(10)$ or high-energy fluence ($E > 20$ MeV) were obtained in a comparison organized at the GSI by CONRAD (COordinated Network for RAdiation Dosimetry, 6th Framework Programme), where different ERBSSs and ERRCs were exposed in the neutron field produced by a 400 MeV/A carbon beam on a graphite target, after a thick concrete wall [26].

As a conclusion, it is reasonable to expect that well-established ERBSSs, exposed in a broad field including a high-energy component as at CERF, are able to provide the spectrum-integrated quantities with system-to-system differences lower than 10%. In addition, similar differences may be found between the Monte Carlo simulation and the experimental values.

For the ERRCs the response function does not reproduce exactly the fluence-to-$H^*(10)$ conversion coefficients. In others words the response function in term of ambient dose equivalent $H^*(10)$ is not exactly flat. This fact is particularly important if the calibration conditions are very different from the measuring ones. This source of uncertainty, together with the above consideration about the Monte Carlo reliability permits to conclude that differences of the order of 20–25% between ERRCs, other instruments such as ERBSSs or results of Monte Carlo simulations are not surprising and acceptable for operational radiation protection purposes.

3. Experimental

Of the four ERBSSs employed in this experiment, three were active systems, two employing a ^{3}He proportional counter as thermal detector and one a LiI(Eu) scintillator. The fourth ERBSS used a CR-39 nuclear track detector coupled to a boron converter as neutron sensor. The four systems are briefly described below.

3.1. CERN active ERBSS

The CERN ERBSS [6] consists of seven spheres, five made of polyethylene with outer diameters of 81 mm, 108 mm, 133 mm, 178 mm and 233 mm. The other two (conventionally named Stanlio and Ollio), are polyethylene spheres with cadmium and lead inserts to extend the response of the BSS to high-energy neutrons. The smallest sphere (81 mm) can be used both bare and enclosed in a cadmium shell of 1 mm thickness in order to impose a cut-off in the thermal response, thus acting as eighth detector. For the present measurements the system was complemented by the LINUS rem counter [4,5,27], used as ninth detector.

The BSS uses a Centronic SP9 spherical ^{3}He proportional counter with diameter of 33 mm located in a cavity at the center of each sphere (http://www.centronic.co.uk/helium.htm). The counter is homogeneously filled with $p=202.65$ kPa ($=2$ atm) ^{3}He and $p=101.325$ kPa ($=1$ atm) krypton gas. The detector is powered to 890 V and it is coupled to a ORTEC 142IH preamplifier, a ORTEC 570 amplifier, a Ortec 550A single channel analyzer (SCA), a Ortec 994 counter, all assembled in a portable NIM crate. A personal computer (PC) based multichannel analyzer, MCA Adcam ORTEC 926, is used to visualize the spectrum of the recoils in the ^{3}He gas, acquired with the "MAESTRO" software. The LINUS uses the same type of ^{3}He proportional counter and the same electronics but a different operating voltage and different value of the SCA lower level.

The response functions of the BSS were calculated by Monte Carlo simulations with the FLUKA98 code, the FLUKA [15,16] version available at that time [6,28,29]. The neutron response of each detector was calculated for 78 incident neutron energies. For $E_n=0.05$, 0.1, 0.25, 0.5, 1 and 2 GeV, a broad parallel beam having extension slightly larger than the sphere diameter was assumed. Since in most measurement conditions low energy neutrons arise from down-scattering and are undirectional, an isotropic distribution of the incident neutrons was chosen for the FLUKA 72 low-energy groups, between $E=19.6\times10^6$ eV and 1×10^{-5} eV. It was assumed that each ^{3}He(n,p)t event is registered and contributes to the reading of the Bonner sphere. The proton as well as the tritium contributes to the detector signal, their combined energy being $E=764$ keV (Q-value) plus the kinetic energy of the incident neutron. The elastic cross-section can be neglected for the given problem, because it is more than three orders of magnitude smaller at thermal energies and still more than two orders of magnitude smaller at 1 eV [30].

Each detector response has a maximum at a certain energy which depends on the moderator size and shows a broad shape at lower energies for the smaller spheres, which gets narrower with increasing diameter whilst the maximum shifts to higher energies. The response matrix was experimentally validated with monoenergetic neutrons and with Am–Be source neutrons, yielding a calibration factor $f_c=1.096\pm0.012$. An overall uncertainty of 5% was assumed for the response matrix.

3.2. POLIMI active and passive ERBSS

The POLIMI ERBSS is a modification of the one described in Ref. [31]. It is composed of seven spheres designed to host at its center either active or passive thermal neutron detectors. Five spheres are made of polyethylene with outer diameters of 81 mm, 108 mm, 133 mm, 178 mm and 233 mm. The sixth is an 81 mm polyethylene sphere surrounded by an outer lead shell 2 cm thick. The seventh, which also acts as an ERRC, is a polythene sphere with lead and cadmium insets. The sphere has a 12.5 cm outer radius: an inner 5.6 cm radius polythene sphere is surrounded by a 6 mm thick lead shell; the outer part of the inner sphere hosts eleven cadmium buttons 2.5 cm in radius and 1 mm in thickness [32].

The active thermal neutron detector is a Centronic SP9 spherical ^{3}He proportional counter with filling pressure of 4 atm (http://www.centronic.co.uk/helium.htm). The passive detector is made of two PADC track detectors (supplied by Intercast Europe, Parma, Italy) [33] coupled with a boron converter. The tracks are produced via (n,α) reactions in ^{10}B. In order to maximize the detector sensitivity an enriched boron converter (99% ^{10}B) supplied by DosiRad (Lognes, France) was used.

As for the rem counters (in the following referred to as either active ERRC or passive ERRC, according to the detector used), the response function was calculated for the two thermal neutron detectors. The results [32] show a very smooth difference in the two response functions. For the other spheres the response function was calculated for the passive detector only and also used for the active one. An analysis of the variation of the response function for a similar ERBSS hosting an active/passive detector can be found in Ref. [31]. This simplification can introduce an uncertainty especially for the smaller spheres. The spheres were not calibrated individually and give an output spectrum in arbitrary units. The ERRC (the 7th sphere), calibrated with a Pu–Be neutron source at the CERN calibration facility, is used to measure the value of ambient dose equivalent directly.

The PADC detectors are etched for 40 min at 98 °C in a 7.25 M NaOH aqueous solution. Under these conditions the bulk etching velocity is 10 ± 0.5 μm/h corresponding to a removed layer of 6.6 ± 0.4 μm. The detectors are analyzed using the Politrack track detectors reader [34]. This reader permits to measure several track parameters, some of which are used to calculate the LET of the particle that produced the track. Fig. 1 shows the frequency distributions of the track minor axis, the track area, the V ratio (the ratio between the track etching velocity V_t and the bulk etching velocity V_b) and the LET distribution.

The first peak in the minor axis and area distributions is due to the alpha particles while the second one is due to the lithium ion. The mean LET distribution is calculated starting from the V distribution: it shows a sharp peak at about 220 keV/μm that is in very good agreement with the mean LET calculated as the alpha particle energy (1470 keV) divided by the range in the PADC detector (6.15 μm) calculated with SRIM2010 [35]. The second peak is due to the lithium ions. In this case, according to the fact that the tracks are heavy overetched, the measured mean LET overestimates by about a factor of 2 the lithium mean LET. This overestimation has no impact on the detector analysis because

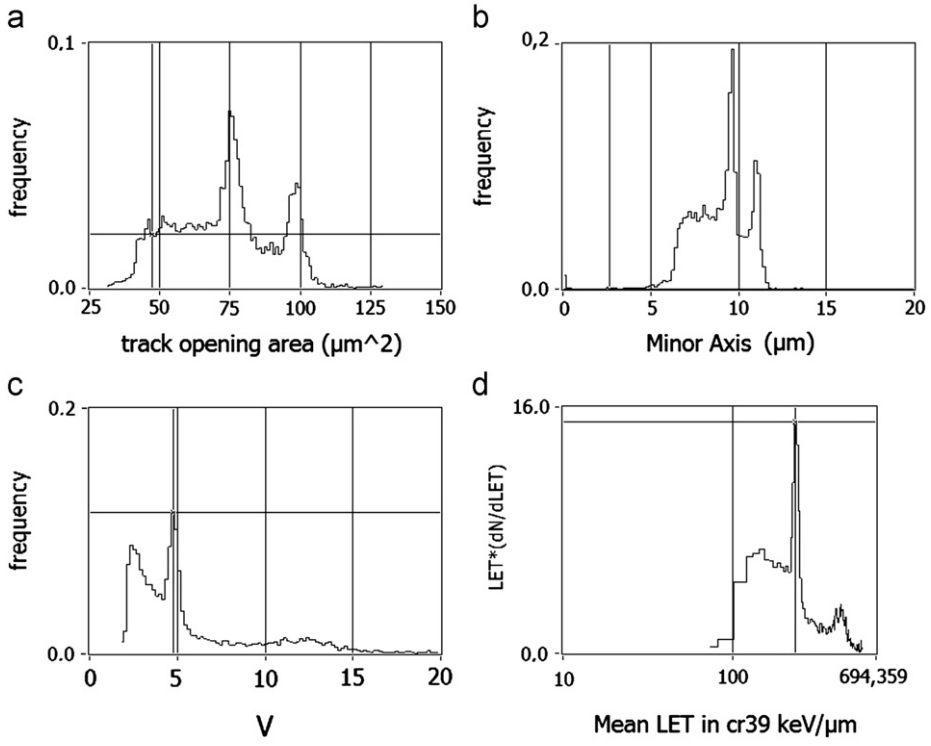

Fig. 1. Distributions of track and particle parameters. See text for details.

the interest is in track counting only. The above described distributions are only used to set regions of interest encompassing the signal and thus improving the signal to noise ratio.

3.3. INFN active ERBSS

The INFN BSS [10,36] is made up of seven polyethylene (PE) spheres, with their diameters labeled in inches (2 in., 3 in., 5 in., 7 in., 8 in., 10 in., and 12 in.) for convenience, plus three high-energy spheres, called ERS-1, ERS-2 and ERS-3 having the following composition:

LNF-ERS-1: external diameter 7 in.; it includes an internal 4 in. PE sphere surrounded by 1.27 cm of lead;
LNF-ERS-2: external diameter 7 in.; it includes an internal 4 in. PE sphere surrounded by 1.27 cm of copper;
LNF-ERS-3 external diameter 12 in.; it includes an internal 3.15 in. PE sphere surrounded by 1 cm of lead.

The central thermal neutron detector is a cylindrical $4\,\text{mm}\times 4\,\text{mm}$ ^{6}LiI(Eu). The response matrix, calculated with MCNPX [14] for 120 logarithmic equidistant discrete energy values between 1.5×10^{-9} MeV and 1.16 GeV, was validated in radionuclide [37] or quasi mono-energetic neutron reference fields [38]. Its overall uncertainty, found to be $\pm 3\%$, was estimated on the basis of these irradiations as the relative standard deviation of the ratio between the measured counts and those expected by folding the response matrix with the tabulated spectra. The calibration factor of the ERBSS is verified every two years by exposing the large spheres (5 in. and larger) to a NPL-calibrated ^{241}Am–Be source (the source strength is known within less than $\pm 1\%$). As a routine quality assurance programme, the efficiency of the central ^{6}LiI(Eu) detector is checked, before and after an experimental campaign, using a fixed-geometry portable moderator with a small (3.7 GBq) ^{241}Am–Be source in its center. As a result, the spectrometer calibration factor is known within less than $\pm 2\%$ uncertainty.

The INFN ERBSS was recently used in neutron fields with significant high-energy component ($E>20$ MeV), such as the ANITA neutron beam at TSL Uppsala [25] and the forward-directed stray field produced by a 62 MeV proton beam on a PMMA target, at the INFN-LNS hadrotherapy facility [39]. In both cases the estimation provided for the high-energy component was coherent with reference data (TSL) or the data provied by other well-established ERBSS (INFN-LNS).

4. Measurements

CERF is a reference radiation facility in operation at CERN since several years, providing a neutron spectral fluence typical of that normally encountered outside high-energy proton accelerator shields and similar to the radiation environment at commercial flight altitudes [13]. The stray radiation field is created by a positive hadron beam (mixed 1/3 protons and 2/3 pions) with momentum of 120 GeV/c incident on a cylindrical copper target (7 cm in diameter and 50 cm in length) placed inside an irradiation cave. The target is shielded on top by 80 cm thick concrete. This roof shield produces an almost uniform radiation field over an area of 2×2 m^2, divided into squares of 50×50 cm^2 providing 16 reference exposure locations (concrete top, CT) where the neutron energy distribution is known by Monte Carlo simulations and past measurements. Here the neutron spectral fluence is characterized by a thermal peak with energy around 4×10^{-7} MeV, an intermediate region between the thermal and the evaporation peak, placed at about 1 MeV, and by a high-energy peak centered at about 100 MeV. As stated earlier, the evaporation peak comes from neutrons evaporating from highly excited nuclei, while the high energy peak is due to a broad minimum in the corresponding neutron cross-section at energy of about 100 MeV. The primary beam is monitored by an air-filled

Precision Ionization Chamber (PIC) at atmospheric pressure. One PIC-count corresponds (within $\pm 10\%$) to 2.2×10^4 particles impinging on the target.

The measurements were performed at the end of July and in the beginning of August 2010 in positions CT7 and CT9. The SPS cycle was 45 s with spill length of 9 s. The PIC counts were read out on-line with a Lab-View (National Instruments) program running on a PC. The PIC serves to normalize the experimental counts of each Bonner sphere to the number of particles in the H6 beam hitting the copper target in the CERF irradiation cave. All measurements were performed by placing each sphere in the given location (CT7 or CT9) with a sufficient reproducibility. All spheres were exposed in turn in both positions under the same conditions and their count rates normalized to the PIC counts.

The $H^*(10)$ in the two positions was measured with three ERRC of the LINUS type, in order to compare it with the values obtained by the unfolded BSS spectra: the original extended-range rem counter LINUS [4,27,5] in use at CERN and two recent units built by POLIMI [32], one active (employing the same type of proportional counter used in the CERN LINUS and in two of the BSS, the Centronics SP9) and one passive (using a CR-39 track detector coupled to a boron converter), as explained above.

All results presented in Section 6 are normalized per PIC count.

5. Data unfolding

All information from a BSS measurement are contained in the measured count rates and in the response matrix of the spectrometer. The spectral fluence can be evaluated with an appropriate unfolding code that solves the Fredholm integral:

$$C_i = \int_{E_{\min}}^{E_{\max}} f_{i,e} \Phi_E \, \mathrm{d}E + \varepsilon_i \quad (1)$$

in which C_i are the number of counts measured by detector i, $f_{i,e}$ is the response function of the ith detector, Φ_E is the neutron spectrum in the specific energy range defined by $E_{\min}$ and $E_{\max}$ and ε_i is the measurement error in detector i. Several codes employing various mathematical techniques have been developed to perform spectrum unfolding for multisphere systems. Due to the non-uniqueness of the unfolding process, many different methods based on different mathematical principles exist, such as the least-squares iteration, the non-linear least squares methods and the maximum entropy.

The unfolding problem in Bonner sphere spectrometry is under-determined, because the number of mathematical functions that could reproduce a given set of measured sphere counts is theoretically infinite. In principle, the spectrometric information increases as the number of spheres increases, but the amount of added information decreases for each added sphere, because the response functions are partially inter-dependent.

Because the different response functions of a BSS exhibit similarities and superpositions, the energy resolution of the system is known to be poor, especially in the epithermal region. As far as the high-Z loaded spheres are concerned, their response functions tend to be parallel in the high-energy domain ($E > 20$ MeV), thus limiting the amount of spectrometric information obtainable with this technique. Practical consequences are that:

(1) two or three extended range spheres are enough to extract the maximum amount of available information. It is therefore advisable, more than increasing the number of spheres, to investigate new detectors characterized by different shape in their high-energy response;

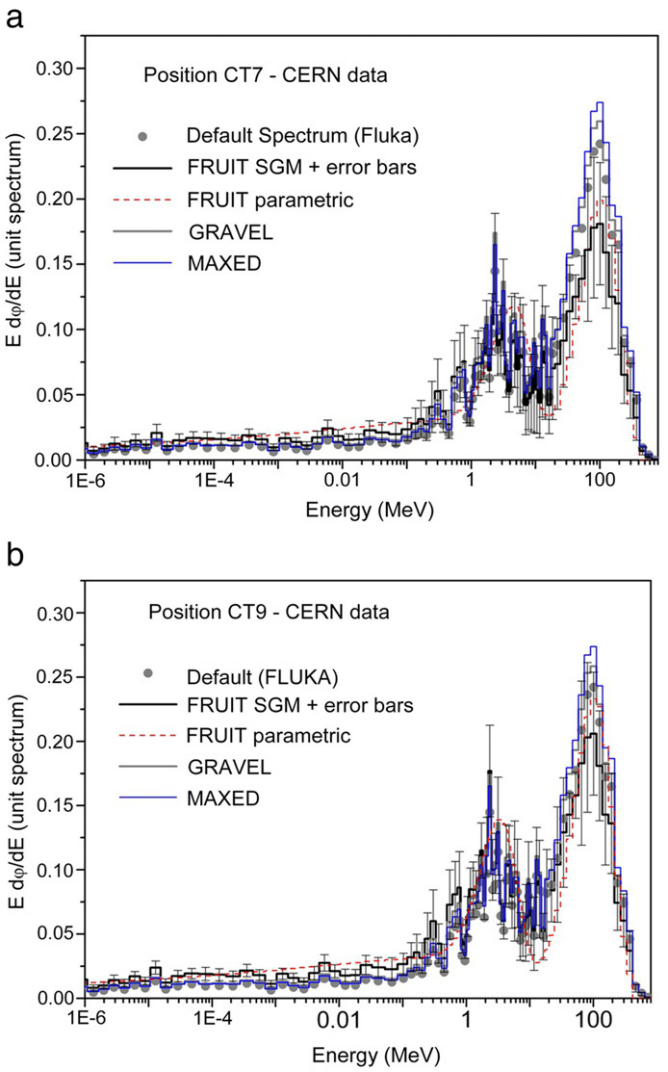

Fig. 2. CERN BSS spectra in the CT7 (a) and CT9 (b) positions. Spectrum simulated by FLUKA and experimental spectra obtained with four unfolding methods: FRUIT (parametric approach), FRUIT (SGM, with uncertainty bars), GRAVEL and MAXED.

(2) the pre-information plays a crucial role in this energy domain. Physically meaningful hypotheses must be formulated to supply the lack of information. As an example, when the measurement point is located behind a thick shield of a high-energy hadron accelerator, the high-energy component can be described by a maxwellian-shaped peak at about 100 MeV.

Provided that a significant amount of pre-information is always required in order to obtain physically meaningful results, several unfolding codes providing pre-information in different ways have been developed. An excellent review of unfolding algorithms can be found in Ref. [40]. More recent unfolding codes are described in Refs. [20,41–46].

Here only a brief discussion is given with the idea to characterize the unfolding codes used in this study. In most cases a default spectrum (DS) is needed. This is typically derived with Monte Carlo simulations and should be as close as possible to the "true" spectrum. The unfolding code iteratively alters this spectrum attempting to reach a good agreement between the experimental counts and the "folded" counts, i.e. those obtained by folding the response matrix with the "candidate" spectrum. Of the many numerical rules used to iteratively alter the spectrum, the maximum entropy principle [47], implemented in the MAXED

code [48], is well-established and known to respect the information contained in the DS to the maximum extent. In addition, the code IQU of the UMG package can be used to do a sensitivity analysis and calculate integral quantities, their uncertainties and a correlation matrix, thus providing estimates of uncertainties in the linear approximation.

When a detailed DS is not available, as it may happen with some operational scenarios, the knowledge of the physical processes at the basis of the neutron emission can be of great help. This is the idea behind the so called parametric codes, which model the neutron spectrum as a superposition of elementary spectra covering the whole energy range and reflecting the neutron producing mechanisms. The neutron spectrum is completely modeled using a reduced number (less than 10) of physically meaningful parameters, whose values are iteratively determined on the basis of the agreement between experimental and "folded" counts. Parametric codes currently in use are FRUIT [20,46] and NUBAY [49]. FRUIT performs statistical analyses to provide probability distributions and confidence intervals for the parameters describing the neutron spectrum. In its latest release (ver. six), the code provides uncertainties for each bin of the neutron spectrum. NUBAY is a Bayesian parameter estimation program that provides posterior probabilities.

Combinations of different codes are frequently used. As examples, the outcome of the NUBAY code has been used as DS for MAXED [50]. Alternatively to the parametric approach, the FRUIT code embeds an option allowing the parametric spectrum (or any spectrum provided by the user) to be used as a DS for a special

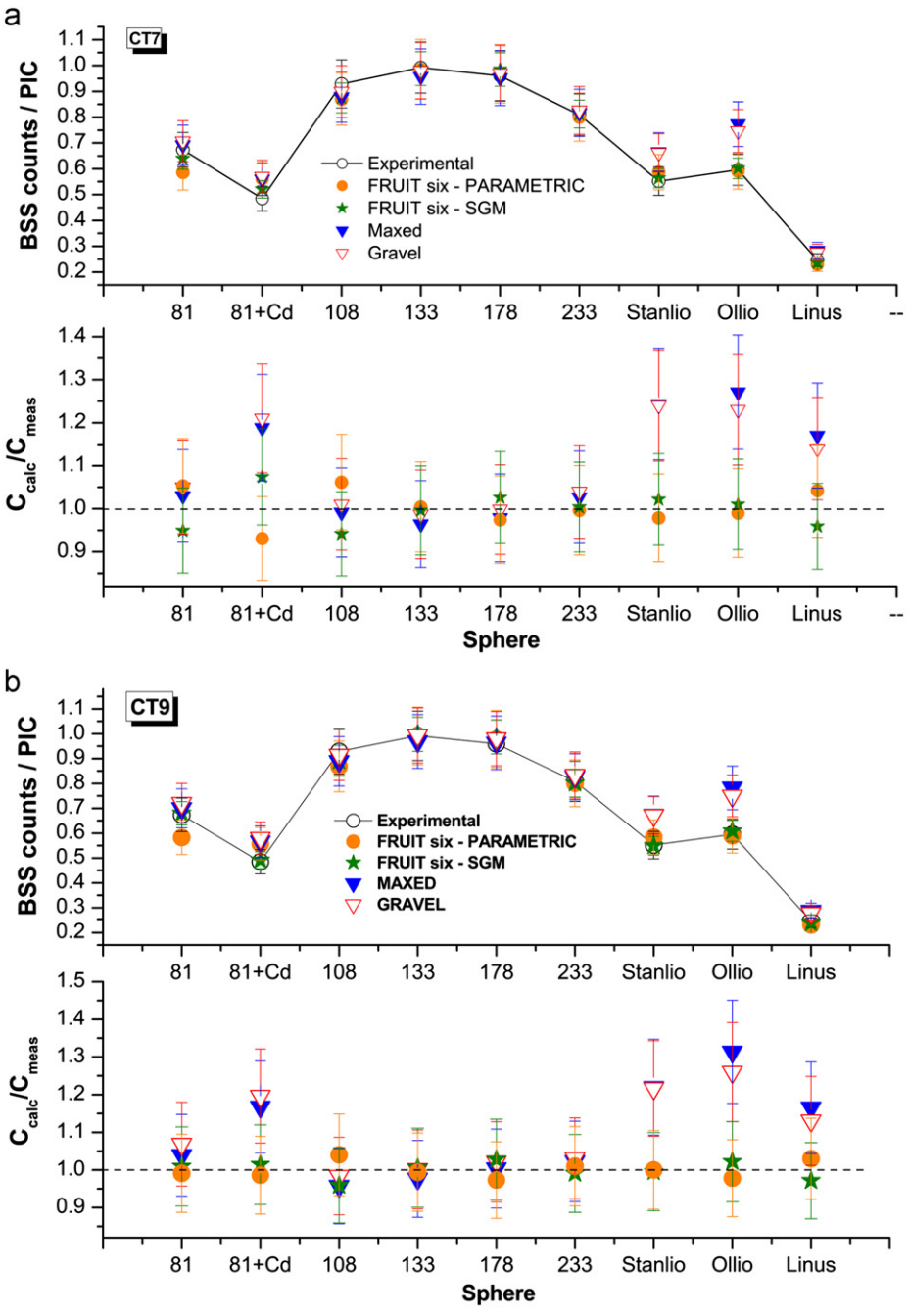

Fig. 3. CERN BSS spectra in the CT7 (a) and CT9 (b) positions. Top figures: experimental versus calculated counts obtained with the two FRUIT models, parametric and numerical, MAXED and GRAVEL. Bottom figures: ratio of calculated to measured counts obtained with MAXED, GRAVEL and FRUIT, parametric and numerical.

gradient algorithm (SGM) similar to that included in GRAVEL [51]. This option is called FRUIT/SGM

In this work the neutron spectra were determined using the MAXED, GRAVEL and FRUIT unfolding codes, being representative of DS-based or parametric codes. MAXED and GRAVEL belong to the PTB U.M.G. package [52]. They are adjustment codes requiring some "a priori" information, which is included in the default spectrum.

MAXED (MAXimum Entropy Deconvolution) [48,53] is a computer program developed to apply the maximum entropy principle to the unfolding of neutron spectrometric measurements. The code makes use of the estimated variances for the count rate of each detector in the unfolding process, appropriately weighting the data from each detector. The algorithm leads to a solution spectrum that is always a non-negative function; the solution spectrum can be written in a closed form. GRAVEL is a modification of SAND-II [52]; it is an iterative algorithm that provides a "free-form" solution (i.e. the solution spectrum does not have to fit any predetermined parametrization of the spectrum), which depends however to some extent on the prior information (i.e. the initial estimate) used.

FRUIT (FRascati Unfolding Interactive Tool) is a parametric code written using the Lab-View software. It models the neutron spectra with at most nine numerical positive parameters. Provided the response matrix and the energy binning, the only numerical data required by the code are the Bonner sphere readings and their relative uncertainties. According to the radiation environment specified by the user, the code selects the appropriate physical model to unfold the experimental data. On the basis of the chosen radiation environment the code generates itself the default spectrum needed to start the iterative procedure. Taking advantage of an adaptative tolerance converge mechanism, the results do not depend on the numerical values of this initial spectrum [46]. The parametric approach may be very convenient in a variety of operational scenarios, especially if detailed a priori information is not available. By contrast, when the final spectrum is likely to be obtained by slightly perturbing a highly reliable "default" spectrum, the traditional "pure mathematical" convergence methods may be used with accurate results. For this purpose the FRUIT code, as an alternative to the parametric approach, includes an unfolding option that perturbs a default spectrum according to a special gradient method (SGM) [39,51]. It this work both the parametric and the SGM algorithms have been employed.

6. Results and discussion

The neutron spectra were deduced from the experimental data using MAXED, GRAVEL and FRUIT (parametric and SGM) for the four systems in the CT7 and CT9 positions. The FRUIT code/parametric mode was used choosing the "high energy hadron accelerator" radiation environment. For MAXED, GRAVEL and FRUIT/SGM mode, the FLUKA spectrum [13] was used as guess spectum.

6.1. Code comparison

6.1.1. CERN data

The solution spectra obtained by unfolding the CERN BSS data with MAXED, GRAVEL and FRUIT/SGM are shown in Fig. 2 as lethargy plots together with the FLUKA reference spectrum [13] used as default spectrum. Fig. 3 compares the experimental counts with the counts obtained by folding the resulting spectra with the ERBSS response matrix. Uncertainty bars on a bin-per-bin basis are available as standard result in both FRUIT modes but, for a better readability, they are only shown for the SGM mode. Because the magnitude of these bars can be regarded as a rough indicator of the resolving power of the spectrometer, it is interesting to note their value: higher than 20% in the eV region; $>20\%$ for $E<10$ MeV; $>30\%$ for $E>10$ MeV. These uncertainties are the result of the propagation of the uncertainties on the input data, σ_{in} (quadratic combination of the BSS counting uncertainty and overall uncertainty of the response matrix), through the unfolding procedure. This propagation is done by randomly generating a large number ($>10^3$) of sets of BSS counts, using σ_{in} as amplitude of the Gaussian perturbation, and then separately unfolding each set. The uncertainties are obtained from the distribution of the results.

For MAXED and GRAVEL, the plotted solution spectrum is the one obtained using the energy bin structure of the response function. Both codes allow changing the energy binnings used for the unfolding: the user can choose either a fine energy bin structure, four bins per decade, the energy bin structure of the default spectrum or the energy bin structure of the response functions. The one chosen offers the best energy representation.

The total experimental uncertainties on the BSS counts were estimated at 12%, which include the statistical uncertainties on the counts, the uncertainty on the response matrix and other factors such as reproducibility of the positioning of each sphere in the exposure location.

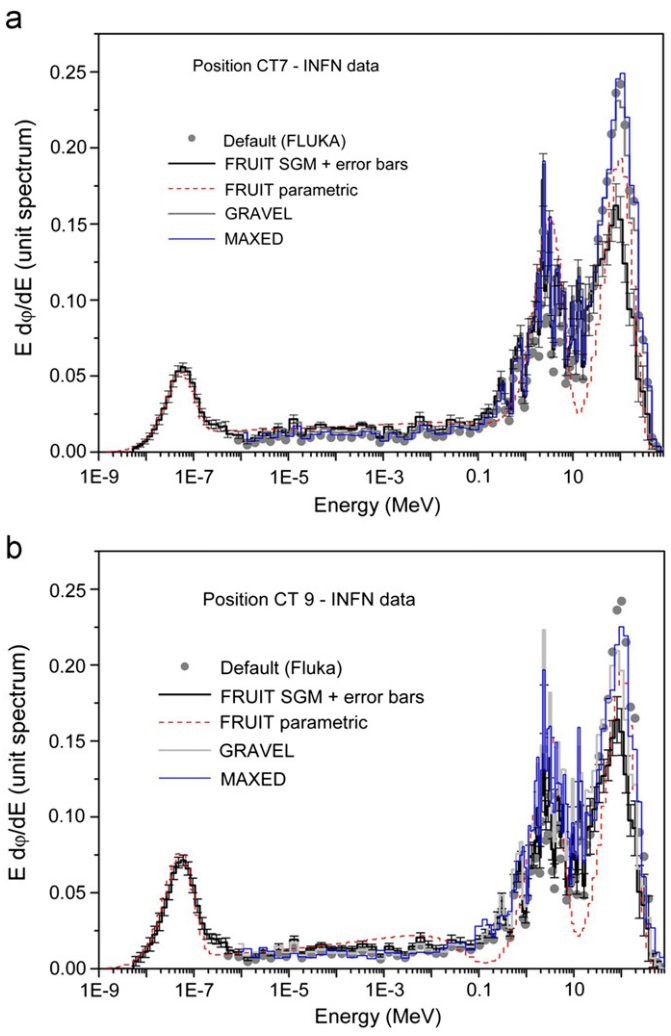

Fig. 4. INFN-LNS BSS spectra in the CT7 (a) and CT9 (b) positions. Spectrum simulated by FLUKA and experimental spectra, obtained with four unfolding methods: FRUIT (parametric approach), FRUIT (SGM, with uncertainty bars), GRAVEL and MAXED.

One sees that there is a general good agreement among the codes, which well reproduce the shape of the default spectrum and are able to correctly position both the high-energy peak and the evaporation peak. The different spectra are in practice superimposed, uncertainty bars taken into account, below 10 MeV. A larger scatter is observed in the height of the high-energy peak. Particularly the MAXED and GRAVEL codes, that are known to respect the pre-information to the maximum extent, are closer to the FLUKA spectrum than the FRUIT results. By contrast, the lower height of the high-energy peak as provided by both FRUIT modes is more respectful of the experimental BSS counts, as evidenced in Fig. 3 (lead-loaded spheres Stanlio and Ollio). On the other hand the uncertainties are rather large in this energy region, and all spectra would be judged comparable if the FRUIT error bars were associated to all spectra, which is a reasonable hypothesis. Fig. 3 confirms that the FRUIT solutions are highly coherent with the experimental counts (maximum deviation about 5–6%), whilst deviations as high as 20–30% are observed for the other codes. The overestimate of the high-energy peak by MAXEL and GRAVEL as compared to FRUIT also explains the overestimate in the

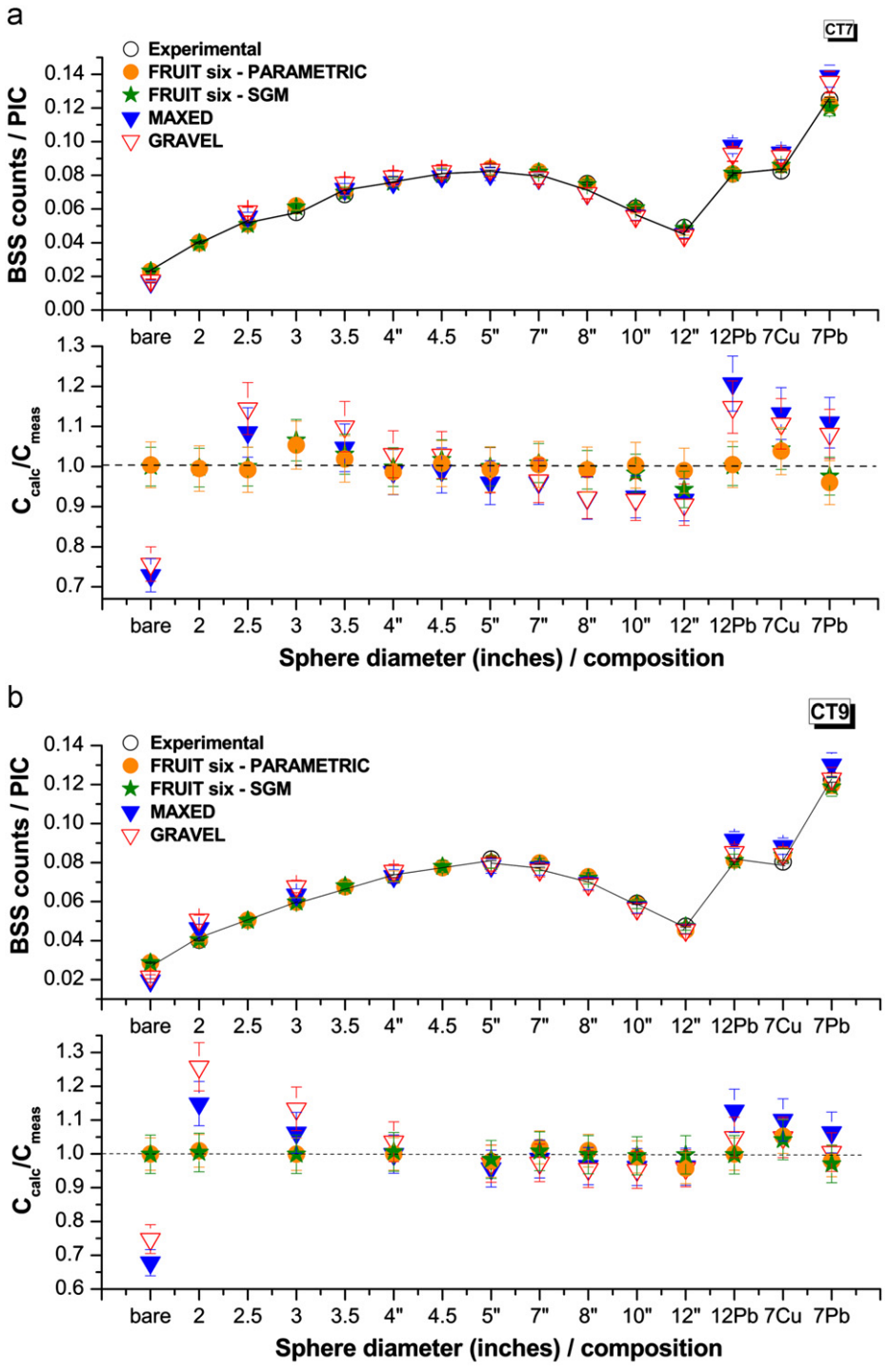

Fig. 5. INFN-LNS BSS spectra in the CT7 (a) and CT9 (b) positions. Top figures: experimental versus calculated counts obtained with the two FRUIT models, parametric and numerical, MAXED and GRAVEL. Bottom figures: ratio of calculated to measured counts obtained with MAXED, GRAVEL and FRUIT, parametric and numerical.

calculated counts from the former codes for Stanlio, Ollio and LINUS (Fig. 3), the three BSS detectors mostly sensitive to the high-energy component of the spectrum.

6.1.2. INFN data

The unfolded spectra from the INFN data are shown in Fig. 4 in the form of lethargy plots, together with the FLUKA spectrum [13]. Fig. 5 compares the experimental sphere counts with the counts obtained by folding the resulting spectra with the ERBSS response matrix. As above, the uncertainty bars specified on a bin-per-bin basis (reported for the FRUIT/SGM only) are useful to evaluate the ERBSS resolving power. Their value is 10–20% for $E<10$ keV; 10–15% for $10\ \text{keV}<E<10$ MeV and $\approx 10\%$ for $E>10$ MeV.

All codes (MAXED, GRAVEL, FRUIT/parametric and FRUIT/SGM) provide comparable results for $E<10$ MeV. The scatter observed in the height of the high-energy peak is more evident than in the case of the CERN data, because the uncertainties of the INFN system are lower than those of the CERN system. The MAXED and GRAVEL spectra are close to the FLUKA spectrum even in the high-energy domain, whilst FRUIT tends to provide less high-energy neutrons. Again, the lower height of the high-energy peak as provided by both FRUIT modes is more respectful of the experimental BSS counts, as evidenced in Fig. 5 and especially from the data of the extended range spheres (12 in.+Pb, 7 in.+Pb, 7 in.+Cu).

Fig. 5 confirms that the FRUIT solutions are always coherent with the experimental counts (within the uncertainties on the sphere counts, about 4%). Deviations as high as 20% are observed for the other codes. Referring to Fig. 5, the uncertainties on the experimental counts (1%) are obtained from the quadratic combination of the counting uncertainties and the uncertainty due to the stability of the central counter with time (both lower than 1%). Because the folded counts are obtained as the product of the response function folded with the unit spectrum (overall uncertainty 3%) and the total fluence (~2.5% uncertainty), their uncertainty are in the order of 3–4%.

6.1.3. POLIMI data

The POLIMI unfolded spectra and the results of the data analysis are shown in Figs. 6 and 7 in the same form described in the previous sections. All codes provide comparable results. A comparison between the results of the active and passive ERBSS evidences a better fit for the passive system. This result is expected because, as mentioned above, the response function was calculated for the passive BSS and also used for the active one. Because the active detector (an SP9 proportional counter) is larger than the CR-39 passive dosimeter, the passive spheres have a higher amount of moderating material around the sensor. The difference in the response function is more evident with the smaller spheres because the percentage difference in moderating material is larger. This fact has two consequences:

(a) the sensitivity of the smaller active spheres without lead is overestimated in the thermal energy region and underestimated in the epithermal one;
(b) the sensitivity of the active sphere with lead is underestimated in the epithermal energy region and overestimated at higher energy.

This effect is consistent with the plots in Fig. 6 that evidence an overestimation both of the thermal and the high energy peak for the active BSS.

The ratio of calculated (C_{cal}) to measured (C_{meaus}) counts shown in Fig. 7 evidences the statistical compatibility between calculated and experimental data. A systematic overestimation of

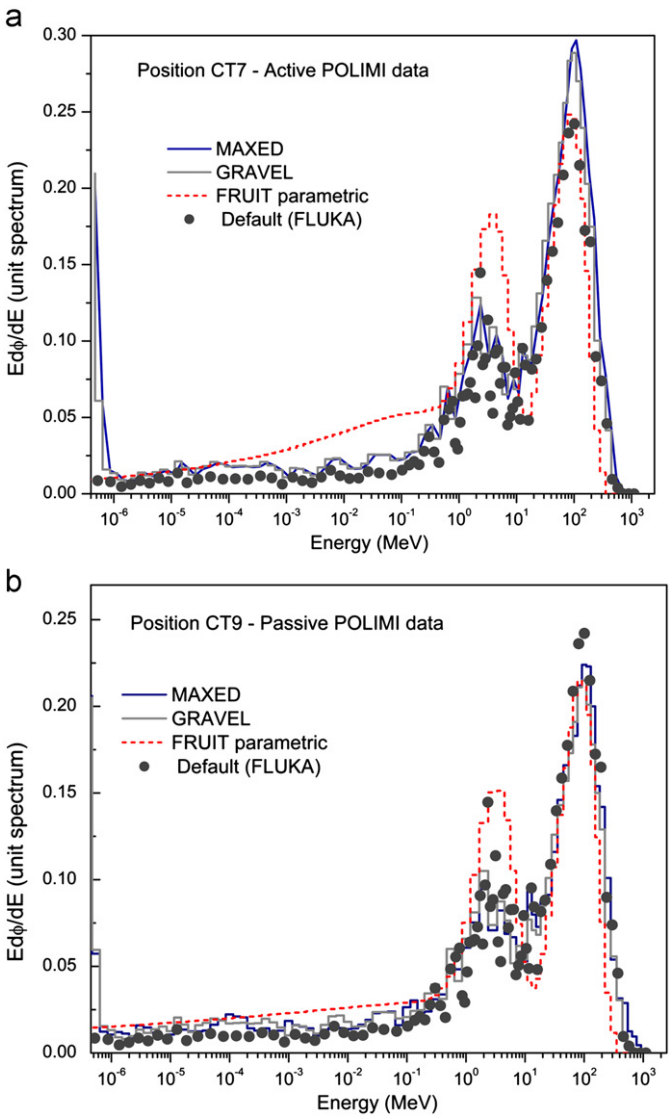

Fig. 6. POLIMI BSS spectra in the CT7 (a) and CT9 (b) positions. Spectrum simulated by FLUKA and experimental spectra, obtained with four unfolding methods: FRUIT (parametric approach), FRUIT (SGM, with uncertainty bars), GRAVEL and MAXED.

the ratio in the lead-loaded spheres can be noted. This effect, which was also observed in the data of the other BSSs, can be explained considering that the unfolding algorithms for all BSSs start from the Monte Carlo default spectrum. The code calculates C_{cal} and iterates until the data are statistically comparable with the measured values. If the default is always the same, the C_{cal} values approach the target values C_{meaus} moving always in the same direction and therefore stopping with a systematic overestimation or underestimation of C_{meaus}.

6.2. BSS intercomparison

This section compares the results of the four ERBSSs in terms of unit spectra (i.e. normalized to unit fluence), because the two POLIMI spectrometers are not calibrated in term of ambient dose equivalent/neutron fluence. In addition, the following quantities are discussed: the spectrum-average-fluence to ambient dose equivalent conversion coefficient, $h^*(10)$, the fluence-average energy, E_φ, and the fractions of neutron fluence comprised in given energy intervals of interest, namely: $E<0.4$ eV (thermal component), $0.4\ \text{eV}<E<10$ keV (epithermal component), $10\ \text{keV}<E<10$ MeV

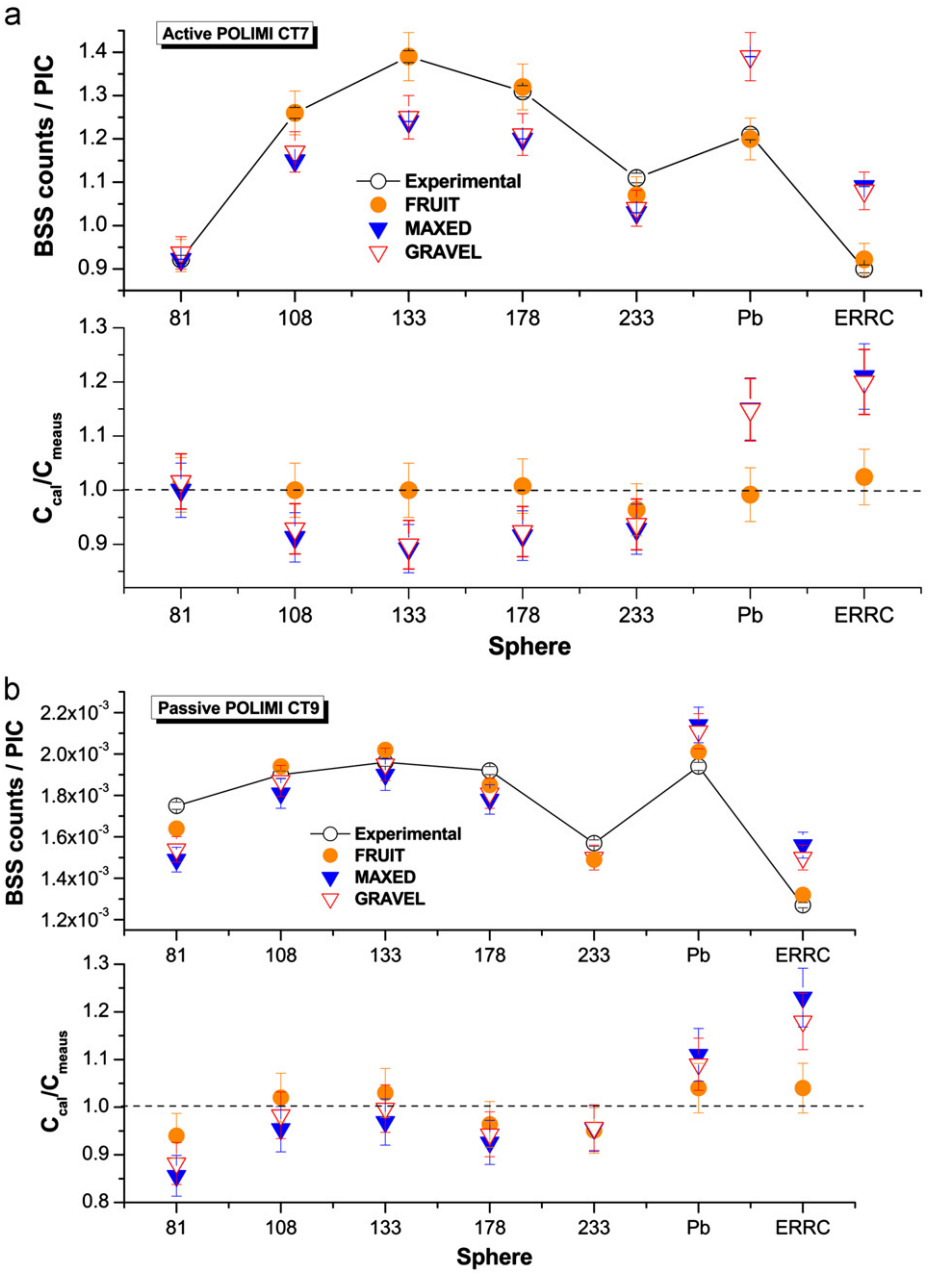

Fig. 7. POLIMI BSS spectra in the CT7 (a) and CT9 (b) positions. Top figures: experimental versus calculated counts obtained with the FRUIT, MAXED and GRAVEL. Bottom figures: ratio of calculated to measured counts obtained with MAXED, GRAVEL and FRUIT.

(evaporative/fast component) and $E > 10$ MeV (high-energy component). Pros and cons of the unfolding algorithms are discussed.

Fig. 8 compares the solution spectra obtained unfolding the four ERBSSs data sets in CT7 with MAXED, Fig. 9 compares the spectra in CT9 unfolded with FRUIT. Apart for the CERN BSS (the response function of which cannot resolve the thermal region because of the FLUKA energy groups), the position of the thermal peak coincides for all BSS but its height varies. The default spectrum used to unfold the INFN data with MAXED was obtained by adding a Maxwellian peak in the thermal region to the FLUKA spectrum.

Unfolding with MAXED and GRAVEL was done with a reduced chi-squared equal to 1.1, which means assuming a good "trust" in the experimental data. Additional unfoldings were made increasing the chi-squared to 2 and 5. The unfolded spectra do not change substantially; the only appreciable difference is that they tend to approach further the guess spectrum, as it can be expected because raising the chi-squared means decreasing the weight given to the experimental data and giving more weight to the guess. The differences in the results with the various unfolding codes mainly depend on the different ways to provide pre-information to the convergence algorithm. In the case of MAXED and GRAVEL a default spectrum derived from Monte Carlo simulations is used, while FRUIT summarizes the relevant physics in terms of a spectrum given in parametric form. Both MAXED and GRAVEL tend to yield a solution spectrum very close to the default spectrum. FRUIT/parametric uses a limited amount of "a priori" information. Because it mainly relies on the response functions, its results always respects the experimental counts. The POLIMI active and passive BSS use the same response functions, which is not fully correct as explained above. Considering that the four spectrometers are made of different numbers of spheres (9 for CERN, 7 for POLIMI and 15 for INFN), fact that also has an influence on the system response, the results of the intercomparison can overall be regarded as satisfactory.

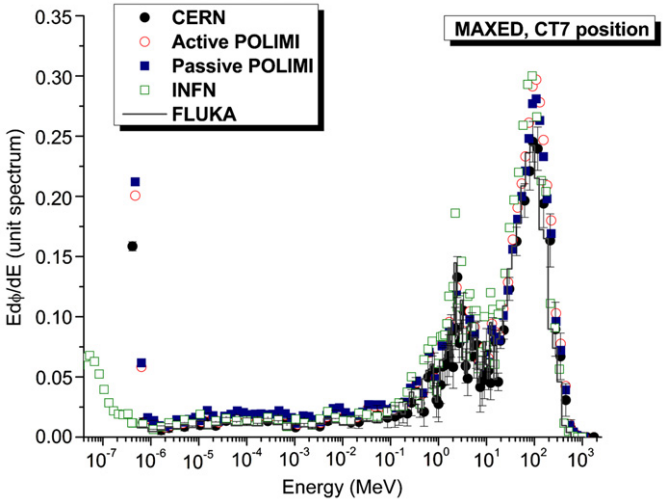

Fig. 8. Comparison of the normalized fluence spectra obtained in CT7 with the four BSS, unfolding the experimental data with MAXED. The FLUKA spectrum is also shown. For the CERN spectrum the error bars were obtained from the estimated uncertainties derived from the FRUIT unfolding. Although obtained with a different unfolding code (FRUIT instead of MAXED), they are nonetheless representative.

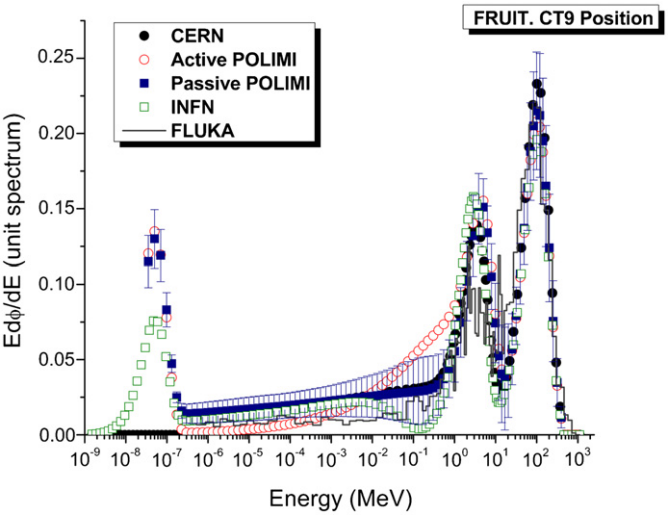

Fig. 9. Comparison of the normalized fluence spectra obtained in CT9 with the four BSS, unfolding the experimental data with FRUIT (parametric). The FLUKA spectrum is also shown.

Fig. 10 compares the fluence spectra obtained in CT7 and CT9 with the CERN and INFN BSS using the FRUIT/SGM mode and the FLUKA spectrum as a guess, derived with independent unfolding procedures. Each spectrum is shown with its uncertainty bars. In the energy range of interest for this study ($E > 0.1$ MeV) these uncertainties are in the order of 20–30% (CERN data) or 10% (INFN data). Being the spectra in good agreement one can conclude that the CERN and INFN systems are compatible.

Table 1 gives the fluence-average energy derived by unfolding the experimental data with FRUIT. The somewhat higher value derived for the CERN BSS is due to the fact that this system cannot resolve the thermal component, as its response matrix was calculated with a former version of FLUKA that had a single neutron group below 0.4 eV. Table 2 lists the fractions of neutron fluence comprised in four energy intervals: $E < 0.4$ eV, $0.4\ \text{eV} < E < 10$ keV, $10\ \text{keV} < E < 10$ MeV and $E > 10$ MeV. The fluence fractions are derived unfolding the experimental data with FRUIT/parametric. There is a reasonable agreement amongst the four systems.

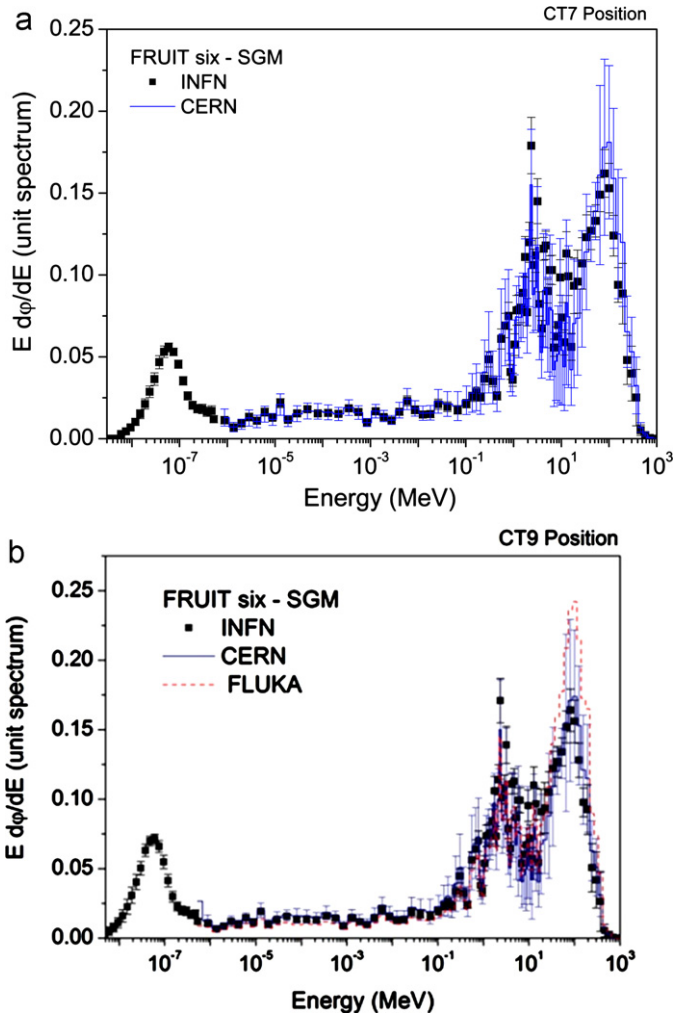

Fig. 10. Comparison between the fluence spectra obtained in CT7 and CT9 with the CERN BSS and the INFN BSS using the FRUIT/SGM, obtained with independent unfolding. In CT9 the results spectra are compared with the FLUKA spectrum used as guess.

Table 1
Fluence average energy derived by unfolding the experimental data with FRUIT.

	Fluence average energy (MeV)			
Location	**CERN**	**POLIMI active**	**POLIMI passive**	**INFN**
CT7	47	38	36	36
CT9	38	33	35	38

The uncertainty associated to the fluence is calculated as the quadratic combination of the unfolding uncertainty and the uncertainty on the spectrometer calibration factor (2% for the INFN BSS, 1.1% for the CERN BSS). The FRUIT unfolding uncertainties are determined via the propagation process described in Section 6.1.1 and can be read from the output file. For MAXED and GRAVEL they are around 10%, corresponding to the relative standard deviation of the counts (the spread of the ratios of the calculated to experimental counts).

The uncertainty for both $h^*(10)$ (the ambient dose equivalent per unit fluence) and $H^*(10)$ is the quadratic combination of the unfolding uncertainty and of the uncertainty on the response matrix, 3% in the case of INFN, 5% in the case of CERN. For POLIMI the uncertainty applies to $h^*(10)$ only and ranges from 8% to 15%

Table 2
Fraction of fluence in four energy intervals derived by unfolding the experimental data with FRUIT. Because the response matrix of the CERN BSS does not resolve the thermal component, this could not be directly estimated (CERN data, 1st line, N.M., not measured). However, to compare them with those obtained with the other three systems, the CERN data were also re-scaled by assuming that the thermal fraction is identical to that measured by the INFN system (CERN data, 2nd line).

BSS	Fluence fraction (%)			
	$E < 0.4$ eV	0.4 eV $< E <$ 10 keV	10 keV $< E <$ 10 MeV	$E >$ 10 MeV
CT7				
CERN	N.M.	17	41	42
	33	11	28	29
POLIMI Active	6	15	43	36
POLIMI Passive	16	15	36	33
INFN	33	6	26	36
CT9				
CERN	N.M.	17	42	41
	35	11	28	26
POLIMI Active	20	7	40	33
POLIMI Passive	22	15	32	31
INFN	35	4	25	36

Table 3
$h^*(10)$ values derived by unfolding the experimental data with MAXED, GRAVEL and FRUIT, parametric and SGM. The reference FLUKA values are also given [13].

	CERN BSS	Active POLIMI BSS	Passive POLIMI BSS	INFN BSS
CT7				
	$h^*(10)$ (nSv cm^2/PIC)			
MAXED	0.28 ± 0.03	0.28 ± 0.03	0.28 ± 0.03	0.27 ± 0.03
GRAVEL	0.28 ± 0.03	0.28 ± 0.03	0.28 ± 0.03	0.26 ± 0.03
FRUIT/par	0.27 ± 0.01	0.32 ± 0.02	0.30 ± 0.03	0.25 ± 0.01
FRUIT/SGM	0.28 ± 0.01			0.27 ± 0.01
Best estimation	0.28 ± 0.01	0.30 ± 0.02	0.30 ± 0.02	0.26 ± 0.01
FLUKA		0.26 ± 0.03		
CT9				
MAXED	0.28 ± 0.03	0.28 ± 0.03	0.27 ± 0.03	0.27 ± 0.03
GRAVEL	0.27 ± 0.03	0.28 ± 0.03	0.27 ± 0.03	0.26 ± 0.03
FRUIT/par	0.27 ± 0.02	0.29 ± 0.03	0.27 ± 0.03	0.25 ± 0.01
FRUIT/SGM	0.27 ± 0.02			0.26 ± 0.01
Best estimation	0.27 ± 0.01	0.28 ± 0.02	0.27 ± 0.02	0.26 ± 0.01
FLUKA		0.25 ± 0.03		

according to the Poisson statistics. The passive system is usually affected by higher uncertainty because of its lower efficiency.

The integral quantities neutron fluence and ambient dose equivalent were also compared. FRUIT provides, with the results of the unfolding, a best estimate of the average value of the spectrum average fluence-to-ambient dose equivalent conversion coefficient $h^*(10)$, of the fluence Φ and of the ambient dose equivalent $H^*(10)$, where $H^*(10)=h^*(10).\Phi$. Both MAXED and GRAVEL do not directly give this type of information, thus these integral quantities were calculated off-line from the unfolded spectra. The $H^*(10)$ was calculated from the neutron spectra obtained with MAXED and GRAVEL via the fluence-to-ambient dose equivalent conversion coefficients for neutrons $h^*_E(10)$ recommended by ICRP [54]:

$$H^*(10) = \int h^*_E(10) \cdot \Phi_E \cdot \mathrm{d}E \qquad (2)$$

Table 3 lists the $h^*(10)$ values for the four BSSs in CT7 and CT9 calculated using the results from MAXED, GRAVEL and FRUIT. For each system, a best estimation was derived by a weighted average of the values given by the different codes. The inverse square of uncertainties were used as weighting factors. All systems provide comparable results and all results compare well with the FLUKA value.

Table 4 gives the fluence values obtained with the three codes for the two calibrated BSS. For each system, a best estimation was also derived by a weighted average of the values given by the different codes. Because the CERN system does not accurately measure thermal neutrons, the two ERBSSs can be properly compared only above 0.5 eV. The table therefore gives both the total fluence and the fluence above 0.5 eV. All results are in rather good agreement. All experimental results also compare well with the Monte Carlo predictions.

Table 5 gives the $H^*(10)$ values obtained with the three codes for the CERN and INFN BSS. For each spectrometer, a best estimation was again derived by a weighted average of the values given by the different codes. The same systematic differences seen in Table 4 are observed here. For both systems the $H^*(10)$ obtained from GRAVEL and MAXED is significantly higher than the FRUIT value. Therefore more neutrons are attributed to the high-energy domain, as in the

Table 4
Fluence values (total and above 0.5 eV) derived by unfolding the experimental data of the CERN and INFN BSS with MAXED, GRAVEL and FRUIT, parametric and SGM. The fluences computed by FLUKA are also given.

	CERN BSS		INFN BSS	
	Total fluence	Fluence above 0.5 eV	Total fluence	Fluence above 0.5 eV
CT7				
	Fluence (1/cm^2/PIC)			
MAXED	0.97 ± 0.09	0.88 ± 0.09	1.20 ± 0.12	1.04 ± 0.10
GRAVEL	0.95 ± 0.09	0.85 ± 0.09	1.18 ± 0.12	1.01 ± 0.10
FRUIT/par	0.84 ± 0.04	0.82 ± 0.04	1.06 ± 0.02	0.91 ± 0.02
FRUIT/SGM	0.88 ± 0.04	0.79 ± 0.04	1.06 ± 0.02	0.91 ± 0.03
Best estimation	0.88 ± 0.03	0.81 ± 0.03	1.07 ± 0.02	0.91 ± 0.02
FLUKA	1.04 ± 0.11	0.89 ± 0.09	1.04 ± 0.11	0.89 ± 0.09
CT9				
MAXED	0.98 ± 0.10	0.89 ± 0.10	1.14 ± 0.13	0.94 ± 0.09
GRAVEL	0.96 ± 0.10	0.85 ± 0.09	1.11 ± 0.12	0.89 ± 0.09
FRUIT/par	0.83 ± 0.04	0.81 ± 0.04	1.08 ± 0.02	0.89 ± 0.02
FRUIT/SGM	0.91 ± 0.05	0.78 ± 0.04	1.08 ± 0.03	0.89 ± 0.03
Best estimation	0.88 ± 0.03	0.81 ± 0.03	1.08 ± 0.02	0.89 ± 0.02
FLUKA	1.01 ± 0.10	0.85 ± 0.09	1.01 ± 0.10	0.85 ± 0.09

Table 5
$H^*(10)$ calculated by unfolding the experimental data with MAXED, GRAVEL and FRUIT for the CERN and INFN systems. The FLUKA reference values are given in Table 6.

	CERN BSS	INFN BSS
CT7		
	$H^*(10)$ (nSv/PIC)	
MAXED	0.27 ± 0.03	0.32 ± 0.03
GRAVEL	0.26 ± 0.03	0.31 ± 0.03
FRUIT/par	0.21 ± 0.01	0.27 ± 0.01
FRUIT/SGM	0.22 ± 0.02	0.29 ± 0.01
Best estimation	0.22 ± 0.02	0.28 ± 0.01
CT9		
MAXED	0.27 ± 0.03	0.30 ± 0.03
GRAVEL	0.26 ± 0.03	0.29 ± 0.03
FRUIT/par	0.23 ± 0.02	0.26 ± 0.01
FRUIT/SGM	0.25 ± 0.02	0.28 ± 0.01
Best estimation	0.25 ± 0.01	0.27 ± 0.01

Table 6
$H^*(10)$ calculated from FLUKA [13] and estimated with three ERRCs.

$H^*(10)$ CERN LINUS (nSv/PIC)	$H^*(10)$ POLIMI active ERRC (nSv/PIC)	$H^*(10)$ POLIMI passive ERRC (nSv/PIC)	$H^*(10)$ FLUKA reference value (nSv/PIC)
CT7 0.23 ± 0.03	**CT7** 0.21 ± 0.03	**CT7** 0.20 ± 0.04	**CT7** 0.27 ± 0.03
CT9 0.22 ± 0.03	**CT9** 0.21 ± 0.03	**CT9** 0.21 ± 0.04	**CT9** 0.25 ± 0.03

FLUKA spectrum used as default spectrum. By contrast FRUIT privileges the agreement between experimental and "folded" counts, thus reducing the high-energy fraction with respect to the FLUKA spectrum. With the idea of respecting both approaches, the weighted average may be considered as a sort of "final decision".

Table 6 provides the "reference" $H^*(10)$ values calculated by FLUKA [13] and measured by the three ERRCs. All rem counters agree well amongst themselves and with FLUKA within their respective uncertainties (although they seem to systematically underestimate the FLUKA predictions by about 25%). These values also compare rather well with the $H^*(10)$ as derived by the BSSs.

7. Conclusions

This exercise presents analogies with the ERBSS inter-comparison organized at the GSI in 2006 in the framework of the CONRAD project [26], where four extended-range Bonner sphere spectrometers from four institutes were used. The main difference is that in the present paper all sets of data were analyzed with all unfolding codes, allowing to some extent to separate the discussion on the different ERBSS from the discussion on the different codes. Another point is that in this exercise the spectra are for the first time reported with uncertainty bars specified bin per bin, and reflecting the degree of validation of the response matrix and the uncertainties in the BSS counts. These bars allow a direct evaluation of the system-to-system compatibility.

As for the 2006 CONRAD exercise, this comparison confirms the capability of an ERBSS to estimate well the integral quantities like fluence and ambient dose equivalent in accelerator-based neutron fields. Particularly, if the ERBSS are well-established (response matrix verified in reference fields and routine application of quality assurance and quality control (QA/QC) procedures), the total fluence may be estimated rather accurately even if different unfolding codes are used. In the present exercise, the values of fluence per PIC (precision ionization chamber)-count estimated with the CERN and INFN ERBSSs with four codes (MAXED, GRAVEL, FRUIT/parametric and FRUIT/SGM) agree reasonably well.

The four BSSs agree very well when compared in term of $h^*(10)$, as shown in Table 3 and Figs. 8 and 9. This comparison is independent of the BSS calibration factor; the uncertainty associated to $h^*(10)$ is lower than the one associated to $H^*(10)$ because it does not embed the calibration uncertainty. Such an approach allows a comparison in more severe conditions (the output quantities to be compared are affected by a lower uncertainty) and permits to focus the attention on the differences among the BSSs and unfolding algorithms.

Higher deviations are expected in the $H^*(10)$ value for fields with a relevant high-energy component. This arises from various reasons: because of the energy dependence of the fluence-to-$H^*(10)$ conversion coefficients, $H^*(10)$ receives an important contribution by the high-energy part of the spectrum ($E > 20$ MeV). In this domain two relevant sources of uncertainties are superimposing:

(1) the simulation codes used to derive the ERBSS response matrix use models that are only partially validated and that imply large code-to-code differences. As stated in Section 2, the impact of such differences on $H^*(10)$ may be in the order of $\pm 10\%$;
(2) due to the poor degree of differentiation in the response function of extended-range spheres, the ERBSS have poor energy resolution in this energy domain.

It is not easy to predict how the two contributions may combine in practice. However, according to a recent experiment performed by the INFN group at TSL (see Section 2), an ERBSS may reasonably estimate the high-energy fluence with 10% accuracy.

The INFN and CERN systems show a good compatibility. This is evident from Tables 4 and 5 and from Fig. 10, where the FRUIT/SGM is applied to both systems, starting from the same guess spectrum (FLUKA), and giving the same resulting spectra. This code tends to respect the guess spectrum only in the position of the structures, i.e. it increases or decreases a given peak on the basis of the experimental counts, but it is unable to create structures which are not included in the guess spectrum.

As a conclusion, all systems are confirmed to be robust and suited for workplace measurements in high-energy fields. All tested unfolding codes are capable to work in high-energy scenarios, but their use should be modulated on the basis of the reliability of the experimental data and of the available pre-information. The unfolding should always be accompanied by a comparison between "measured" and "folded" counts, in order to evidence systematic effects that may arise from the code or the quality of the pre-information.

References

[1] S. Agosteo, M. Silari, L. Ulrici, Radiation Protection Dosimetry 137 (2009) 51.
[2] P. Bilski, J. Blomgren, F. d'Errico, A. Esposito, G. Fehrenbacher, F. Fernàndez, A. Fuchs, N. Golnik, V. Lacoste, A. Leuschner, S. Sandri, M. Silari, F. Spurny, B. Wiegel, P. Wright, in: M. Silari (Ed.), Complex Workplace Radiation Fields at European High-energy Accelerators and Thermonuclear Fusion Facilities, CERN Yellow Report CERN 2006-007, 2006.
[3] R.L. Bramblett, R.I. Ewing, T.W. Bonner, Nuclear Instruments and Methods in Physics Research Section A 9 (1960) 1.
[4] C. Birattari, A. Ferrari, C. Nuccetelli, M. Pelliccioni, M. Silari, Nuclear Instruments and Methods in Physics Research Section A 297 (1990) 250.
[5] C. Birattari, A. Esposito, A. Ferrari, M. Pelliccioni, T. Rancati, M. Silari, Radiation Protection Dosimetry 76 (1998) 135.
[6] C. Birattari, E. Dimovasili, A. Mitaroff, M. Silari, Nuclear Instruments and Methods in Physics Research Section A 620 (2010) 260.
[7] H.H. Hsu, K.R. Alvar, D.G. Vasilik, IEEE Transactions on Nuclear Science NS-41 (4) (1994) 938.
[8] V. Vylet, J.C. Liu, S.H. Rokni, L.-X. Thai, Radiation Protection Dosimetry 70 (1997) 425.
[9] V. Mares, A. Sannikov, H. Schraube, in: Proceedings of the Third Specialists' Meeting on Shielding Aspects of Accelerators, Targets and Irradiation Facilities, Sendai, Japan, 12–13 May 1997, OECD Nuclear Energy Agency, 1998, p. 237.
[10] R. Bedogni, A. Esposito, Nuclear Technology 168 (2009) 615.
[11] G. Leuthold, V. Mares, W. Rühm, E. Weitzenegger, H.G. Paretzke, Radiation Protection Dosimetry 126 (2007) 506.
[12] W. Ruhm, V. Mares, C. Pioch, G. Simmer, E. Weitzenegger, Radiation Protection Dosimetry 136 (2009) 256.
[13] A. Mitaroff, M. Silari, Radiation Protection Dosimetry 102 (2002) 7.
[14] D.B. Pelowitz (Ed.), MCNPX User's Manual Version 2.6.0, Report LA CP-07-1473, 2008.
[15] A. Fassò, A. Ferrari, J. Ranft, P.R. Sala, FLUKA: A Multi-particle Transport Code, CERN-2005-10, INFN/TC_05/11, SLAC-R-773, 2005.
[16] G. Battistoni, S. Muraro, P.R. Sala, F. Cerutti, A. Ferrari, S. Roesler, A. Fassò J. Ranft, in: M. Albrow, R. Raja (Eds.), Proceedings of the Hadronic Shower Simulation Workshop 2006, Fermilab 6–8 September 2006, AIP Conference Proceeding 896, 2007, p. 31.
[17] S. Agostinelli, et al., Nuclear Instruments and Methods in Physics Research Section A 506 (2003) 250.
[18] K. Niita, N. Matsuda, Y. Iwamoto, H. Iwase, T. Sato, H. Nakashima, Y. Sakamoto, L. Sihver, PHITS: Particle and Heavy Ion Transport Code System, Version 2.23, JAEA-Data/Code 2010-022, 2010.
[19] R.E. MacFarlane, in: International Conference on Nuclear Data for Science and Technology, Los Alamos Laboratory, Gatlinburg, Tennessee Preprint, LA-UR-94-1541, 1994.
[20] R. Bedogni, M. Pelliccioni, A. Esposito, Nuclear Instruments and Methods in Physics Research Section A 615 (2010) 78–82.

[21] 〈http://www.eurados.org/〉.
[22] C. Pioch, V. Mares, W. Ruhm, Radiation Measurements 45 (2010) 1263.
[23] Van der Meer, et al., Nuclear Instruments and Methods in Physics Research Section A 217 (2004) 202.
[24] B. Rapp, J.-C. David, V. Blideanu, D. Doré, D. Ridikas, N. Thiollière, in: Proceedings of the Eighth Specialists' Meeting on Shielding Aspects of Accelerators, Targets and Irradiation Facilities (SATIF-8), Pohang, South Korea, 22–24 May 2006, OECD Nuclear Energy Agency, 2010, p. 251.
[25] R. Bedogni, A. Esposito, A. Gentile, Spectrometric Characterization of the Neutron Beam Produced in the ANITA Facility at TSL Uppsala, INFN-LNF-FISMEL Report 01-2011, 2011.
[26] B. Wiegel, S. Agosteo, R. Bedogni, M. Caresana, A. Esposito, G. Fehrenbacher, M. Ferrarini, E. Hohmann, C. Hranitzky, A. Kasper, S. Khurana, V. Mares, M. Reginatto, S. Rollet, W. Rühm, D. Schardt, M. Silari, G. Simmer, E. Weitzenegger, Radiation Measurements 44 (2009) 660.
[27] C. Birattari, A. Esposito, A. Ferrari, M. Pelliccioni, M. Silari, Nuclear Instruments and Methods in Physics Research Section A 324 (1993) 232.
[28] A. Mitaroff, Design, Calibration and Tests of an Extended-Range Bonner Sphere Spectrometer, PhD CERN-Thesis, Technischen Universitat Wien Technisch Naturwissenschaftliche Fakultat, 2001.
[29] E. Dimovasili, Measurements and Monte Carlo Calculations with the Extended-Range Bonner Sphere Spectrometer at High-Energy Mixed Fields, PhD CERN Thesis, EPFL Lausanne, 2004.
[30] Evaluated Nuclear Data File, ENDF/B-VII.1 〈http://www.nds.iaea.org/exfor/endf.htm〉.
[31] M. Caresana, S. Agosteo, F. Campi, M. Ferrarini, A. Porta, M. Silari, Radiation Protection Dosimetry 126 (2007) 314.
[32] S. Agosteo, M. Caresana, M. Ferrarini, M. Silari, Radiation Measurements 45 (2010) 1217.
[33] M. Caresana, M. Ferrarini, M. Fuerstner, S. Mayer, Nuclear Instruments and Methods in Physics Research Section A 683 (2012) 8.
[34] M. Caresana, M. Ferrarini, A. Pola, S. Agosteo, F. Campi, A. Porta, Nuclear Instruments and Methods in Physics Research Section A 620 (2010) 368.
[35] J.F. Ziegler, J.P. Biersack, M.D. Ziegler, SRIM—The Stopping and Range of Ions in Matter, SRIM Co., 2010.
[36] A. Esposito, R. Bedogni, C. Domingo, M.J. García, K. Amgarou, Radiation Measurements 45 (2010) 1522.
[37] R. Bedogni, Ph.D. Thesis, Universidad Autonoma de Barcelona, Barcelona, Spain, 2006.
[38] R. Bedogni, C. Domingo, A. Esposito, M. Chiti, M.J. Garcia-Fusté, G. Lovestam, Nuclear Instruments and Methods in Physics Research Section A 620 (2010) 391.
[39] K. Amgarou, R. Bedogni, C. Domingo, A. Esposito, Nuclear Instruments and Methods in Physics Research Section A 654 (2011) 399.
[40] M. Matzke, Radiation Protection Dosimetry 107 (2003) 155.
[41] M. Tomás, F. Fernández, M. Bakali, H. Muller, Radiation Protection Dosimetry 110 (2004) 545.
[42] B. Mukherjee, Radiation Protection Dosimetry 110 (2004) 249.
[43] H.R. Vega-Carrillo, M.R. Martinez-Blanco, V.M. Hernandez-Dávila, J.M. Ortíz Rodriguez, Journal of Radioanalytical and Nuclear Chemistry 281 (2009) 615.
[44] R. Barquero, R. Mendez, M.P. Iniguez, H.R. Vega-Carrillo, M. Voltchev, Radiation Protection Dosimetry 101 (2002) 493.
[45] H.R. Vega-Carrillo, V.M. Hernàndez-Dàvila, E. Manzanares-Acuña, G.A. Mercado, E. Gallego, A. Lorente, W.A. Perales-Muñoz, J.A. Robles-Rodrıguez, Radiation Protection Dosimetry 118 (2006) 251.
[46] R. Bedogni, C. Domingo, A. Esposito, F. Fernandez, Nuclear Instruments and Methods in Physics Research Section A 580 (2007) 1301.
[47] E.T. Jaynes, Physical Review 106 (1957) 620.
[48] M. Reginatto, P. Goldhagen, Health Physics 77 (1999) 579.
[49] M. Reginatto, Radiation Protection Dosimetry 121 (2006) 64.
[50] K. Amgarou, V. Lacoste, A. Martin, Nuclear Instruments and Methods in Physics Research Section A 629 (2011) 329.
[51] M. Matzke, Unfolding of Pulse Height Spectra: The HEPRO Program System, Report PTB-N 19. Braunschweig: Physikalisch-Technische Bundesanstalt, 1994.
[52] M. Reginatto, The "Few-channel" Unfolding Program in the UMG Package: MXD_FC33, GRV_FC33 and IQU_FC33 (UMG Package, Version 3.3), 2004.
[53] M. Reginatto, P. Goldhagen, S. Neumann, Nuclear Instruments and Methods in Physics Research Section A 476 (2002) 242.
[54] ICRP, Conversion coefficients for use in radiological protection against external radiation, Annals of the ICRP 26(3/4) (1996) (ICRP Publication 74).